ENVIRONMENTAL RESEARCH
LETTERS

LETTER • OPEN ACCESS

Reduction in European anthropogenic aerosols and the weather conditions conducive to $PM_{2.5}$ pollution in North China: a potential global teleconnection pathway

To cite this article: Zhili Wang *et al* 2021 *Environ. Res. Lett.* **16** 104054

ENVIRONMENTAL RESEARCH
LETTERS

OPEN ACCESS

RECEIVED
9 April 2021

REVISED
9 September 2021

ACCEPTED FOR PUBLICATION
14 September 2021

PUBLISHED
19 October 2021

LETTER

Reduction in European anthropogenic aerosols and the weather conditions conducive to $PM_{2.5}$ pollution in North China: a potential global teleconnection pathway

Zhili Wang[1,*], **Jin Feng**[2,*], **Chenrui Diao**[3], **Yanjie Li**[4], **Lei Lin**[5] **and Yangyang Xu**[3]

[1] State Key Laboratory of Severe Weather and Key Laboratory of Atmospheric Chemistry of CMA, Chinese Academy of Meteorological Sciences, Beijing, People's Republic of China
[2] Institute of Urban Meteorology, China Meteorological Administration, Beijing, People's Republic of China
[3] Department of Atmospheric Sciences, Texas A&M University, College Station, TX, United States of America
[4] State Key Laboratory of Numerical Modeling for Atmospheric Sciences and Geophysical Fluid Dynamics, Institute of Atmospheric Physics, Chinese Academy of Science, Beijing, People's Republic of China
[5] School of Atmospheric Sciences and Guangdong Province Key Laboratory for Climate Change and Natural Disaster Studies, Sun Yat-sen University, Zhuhai, People's Republic of China
[*] Authors to whom any correspondence should be addressed.

E-mail: wangzl@cma.gov.cn **and** jfeng@ium.cn

Keywords: aerosol forcing, $PM_{2.5}$ pollution, weather conducive to air pollution, teleconnection

Supplementary material for this article is available online

Abstract

Frequent and severe $PM_{2.5}$ pollution over China seriously harms natural environment and human health. Changes in meteorological conditions in recent decades have been recognized to contribute to the long-term increase in $PM_{2.5}$ pollution in North China (NC). However, the dominant climatic factors driving the interdecadal changes of the weather conditions conducive to $PM_{2.5}$ pollution remain unclear. Here we identify a potential global teleconnection mechanism: the decadal reduction in European aerosol emissions since the 1980s may have partially contributed to the interdecadal increase in weather conditions conducive to $PM_{2.5}$ pollution in NC, measured by an Emission-weighted Air Stagnation Index (ASI_E) that increases at a rate of 6.2% decade^{-1} (relative to the 1981–1985 level). By regression analysis, we show that the decreased European aerosol loadings can warm the lower atmosphere and induce anomalous ascending motion in Europe, which potentially stimulates two anomalous Rossby wave trains in the upper troposphere travelling eastward across Eurasia. The teleconnection patterns project on NC by weakening the near-surface horizontal dispersion, which may be favorable to the increase in local ASI_E and air pollution build-up. The suggested mechanism is further supported by the results from a set of large-ensemble simulations, showing that the European aerosol emission decline since the 1980s excites similar local heating and ascending motion and leads to increasing trends of 0.1–0.5 μg m^{-3} (38 year)$^{-1}$ in surface sulfate concentrations over most of NC. This proposed 'West-to-East Aerosol-to-Aerosol' teleconnection mechanism helps resolve opposite views on the impact of global versus local aerosol forcing on $PM_{2.5}$ pollution weather in NC. The policy implication is that the sustained decline in European aerosol emissions in coming decades, in conjunction with unabated global and regional warming, could further exacerbate air pollution in NC, thus imposing stronger pressure to reduce local emission sources quicker and deeper.

1. Introduction

With rapid economic growth powered by intense fossil fuel (FF) use, China has encountered frequent and widespread air pollution in recent decades (Cai *et al* 2017, Zhang *et al* 2018, An *et al* 2019). Notably the air pollution is due to a dense accumulation of particles with an aerodynamic diameter smaller than 2.5 μm ($PM_{2.5}$) near the ground, and it does great damage to human health (Pope and Dockery 2006, Rich *et al* 2012, Cohen *et al* 2017).

A significant increase in anthropogenic aerosol (AA) emissions is the primary cause of intensified $PM_{2.5}$ pollution (An *et al* 2019). However, the role of meteorology (e.g. horizontal dispersion, and planetary boundary layer (PBL) height) in the formation, accumulation, and dissipation of $PM_{2.5}$ pollution cannot be ignored. Here, we broadly refer to these meteorological conditions as '$PM_{2.5}$ pollution weather'. The effects of $PM_{2.5}$ pollution weather have been clearly demonstrated at daily (Zhang *et al* 2018, Zhong *et al* 2018), seasonal (Wu *et al* 2016), or interannual time scales (Yu *et al* 2019). At the multi-decadal time scale, the focus of this analysis, it has been shown that global warming due to greenhouse gases (GHGs) have significantly contributed to the long-term increase in China's $PM_{2.5}$ pollution weather (Zhang *et al* 2018). The diverse mechanisms involved can include the reduction in surface relative humidity (Ding and Liu 2014), decline in Arctic sea-ice (Zou *et al* 2017), and weakening of the East Asian winter monsoon (Wu *et al* 2016).

But, climate change is not just GHG warming. Historically, AA forcing has imposed a net cooling effect on the climate system (Myhre *et al* 2013), and has been shown to significantly affect tropospheric circulation and global to regional precipitation (Bollasina *et al* 2011). It is less clear how the past changes in AA have affected air pollution related meteorology (i.e. $PM_{2.5}$ pollution weather). This is an intriguing issue because in addition to being a major climate forcing factor, AA is also the air pollutant itself. The mechanism of 'aerosol (forcing) to aerosol (response)', mainly operating at a regional scale in South and East Asia (i.e. well documented interactions between aerosols and monsoon), serves as a key component in the intimately connected chemistry-climate loop (e.g. Lau *et al* 2016). A deeper understanding of how $PM_{2.5}$ pollution weather has changed in the recent past is more than an academic exploration; it is also informative for future policymaking, as governments worldwide are working to reduce local AA emissions to fight air pollution problems. The mitigated emissions will unquestionably contribute to the improvement of local air quality directly. However, it remains unclear whether, *indirectly*, the resultant changes in $PM_{2.5}$ pollution weather at a given location, due to local or remote AA emissions reduction, could enhance or offset the benefit of local AA emissions reduction.

Motivated by this, a limited number of studies focused on $PM_{2.5}$ pollution weather response to AA emission changes, but had provided opposite views (Hong *et al* 2020, Feng *et al* 2020b, Wang *et al* 2021). A recent regional chemistry-climate modeling study demonstrated that future reductions in *local* AA emissions over eastern China would lead to PBL changes that facilitate *vertical ventilation* to improve ground air quality (Hong *et al* 2020). In stark contrast, using large-ensemble experiments from an Earth system model that explicitly include aerosol-cloud interactions, Feng *et al* (2020b) indicated that in response to the decrease in *global* AA emissions, the *horizonal* dispersion would decline, thus worsening the $PM_{2.5}$ pollution weather conditions over eastern China.

Does the difference of the two future-looking modeling studies imply that *non-local* AA forcing far from Asia, such as in Europe, could have a strong influence on $PM_{2.5}$ pollution weather over China? Previous modeling analysis demonstrated that the reduction in European aerosol loadings led to local and Arctic warming (Acosta Navarro *et al* 2016) and exerted major influence on regional meteorology across Eurasia (Liu *et al* 2018, Lewinschal *et al* 2019, Wang *et al* 2020a, 2020b), primarily through changing the mid-latitude jet stream and temperature advection in the upper troposphere.

Here we put this hypothesis to the test by first observationally examining the potential linkage between the European AA reduction and the $PM_{2.5}$ pollution weather in North China (NC) for the period 1981–2018, during which the decrease in sulfur dioxide (SO_2) emissions in Europe was more than two times larger than both the decrease in North America and the increase in Asia (Lamarque *et al* 2010). We also analyze the results from a set of large-ensemble global model simulations, with specific regional AA changes as the single forcing since the 1980s, to further verify the observation-based empirical evidence.

To our knowledge, no *observation-based empirical* studies have been conducted to explore the possible teleconnection between aerosol forcing and aerosol (PM)-related air pollution (a *global* 'aerosol-to-aerosol' connection) operating at a multi-decadal time scale, although there have been ample modeling and observational documentations on such a *local* 'aerosol-to-aerosol' connection operating at a time scale of days to weeks (e.g. Ding *et al* 2016, Gao *et al* 2016, Zhang *et al* 2018, Zhong *et al* 2018). Our findings here can improve the attribution of long-term changes in China's $PM_{2.5}$ pollution and thus better inform policymaking to achieve future clean air goals.

2. Methods

2.1. Observations

The historical SO_2 emissions (up to 2014) from the Community Emissions Data System (CEDS; Hoesly *et al* 2018) were used as a proxy for the temporal trend of AA in Europe, while SO_2 emissions for 2015–2018 were from the Shared Socio-economic Pathway (SSP) 2–4.5 (Rao *et al* 2017, Gidden *et al* 2019). According to Myhre *et al* (2017), European region was defined as 10° W–40° E, 35°–70° N (figure 3(a), box). Note that there were different trends in AA emissions between Western Europe and Central/Eastern Europe. More related to the magnitude of radiative forcing of AA, monthly aerosol optical depth (AOD) from the Modern-Era Retrospective Analysis for Research and Applications, version 2 (MERRA-2) was used. The gridded products of annual surface $PM_{2.5}$ mass concentrations for 1998–2018 derived by combining AOD retrievals from multiple satellites with the Goddard Earth Observing System-Chem chemical transport model (Hammer *et al* 2020) were used here to depict the patterns and trends of $PM_{2.5}$ pollution over China during the past two decades, especially over the hotspot of NC region (defined as 111.9°–119.4° E, 32.5°–41° N; box in figure 7(c)).

To examine the relationship between European aerosols (measured by SO_2 emissions and AOD) and $PM_{2.5}$ concentrations in NC, we conducted regression/correlation analysis on related meteorological variables across Europe and Asia (using the fifth generation European Centre for Medium-Range Weather Forecasts monthly reanalysis (ERA5) data; Hersbach *et al* 2020) and the $PM_{2.5}$ pollution weather (indicated by Emission-weighted Air Stagnation Index, ASI_E, details in the next section). To remove the interference of year-to-year fluctuation and to focus on the multi-decadal trend, all data are smoothed with a five year filter prior to any regression/correlation analysis. Statistical significance is assessed using a two-tailed Student's *t*-test.

2.2. ASI_E

The ASI_E serves as a synthetic meteorological proxy for quantifying the weather conditions conducive to $PM_{2.5}$ pollution. ASI_E is expressed as:

$$\mathrm{ASI_E} = \mathrm{ASI_M}\,(x, y, \mathrm{t}) \cdot \widetilde{E_S}\,(x, y)\,. \tag{1}$$

The ASI_M depends on three key local meteorological factors: precipitation, PBL height, and surface wind speed within the PBL (Feng *et al* 2018), denoted as:

$$\mathrm{ASI_M} = 10^3 \cdot \mathrm{e}^{(1-\delta(r))} \cdot \left(z_{\mathrm{PBL}} - z_0\right)^{-0.75} \cdot \left(\int_{z_0}^{z_{\mathrm{PBL}}} U(z)\,\mathrm{d}z\right)^{-0.25} \tag{2}$$

where $U(z)$ is the wind speed at the geopotential height z (unit: m); z_0 and z_{PBL} are the geopotential heights of the surface and top of the PBL, respectively; r is the daily mean accumulated precipitation rate (unit: mm d^{-1}); and $\delta(r)$ is equal to 1 and 0 for $r \geqslant 1$ and $r < 1$, respectively, depicting the high removing efficiency due to wet deposition. Note that a larger ASI_E values (with smaller surface windspeed, lower PBL height, and lighter precipitation) indicated more favorable weather conditions for the build-up of $PM_{2.5}$ pollution.

$\widetilde{E_s}\,(x, y)$ is the normalized $PM_{2.5}$-related emission factor $E_s\,(x, y)$, which was expressed as:

$$\widetilde{E_s}\,(x, y) = \frac{E_s\,(x, y) - \min\left[E_s\,(x, y)\right]}{\max[E_s\,(x, y)] - \min\left[E_s\,(x, y)\right]} \tag{3}$$

where $E_s\,(\mathrm{x}, y)$ denotes the overall impacts of emissions in grid cell $(x,\ y)$ using the sum of nearby emissions $E\,(x, y)$ weighted by distance and climatological wind fields, and the 'min' and 'max' denote the minimum and maximum of $E_s\,(x, y)$ over NC. E_s includes the emission quantities of SO_2, nitrogen oxides (NO_x), black carbon, organic carbon, terpenes, and other particle sources of $PM_{2.5}$ in the form of:

$$E_s = 0.22E_{s[so_2]} + 0.1E_{s[NO_x]} + E_{s[BC]} + 2.1E_{s[OC]} + 0.17E_{s[terpenes]} + E_{s[OP]}. \tag{4}$$

The ASI_E combines the effects of meteorology and the spatial distribution of emission (time invariant using the present-day level at year 2012). Notably, the time variation in ASI_E depends only on the meteorology according to equation (1); thus, it is a $PM_{2.5}$ pollution weather indictor, rather than direct correspondence of $PM_{2.5}$ level. It has been shown that there are good spatial and temporal relationships between ASI_E and observed $PM_{2.5}$ concentrations over timescales longer than one day (Feng *et al* 2020a).

The daily gridded ASI_E is calculated from the MERRA-2 reanalysis product and then the monthly and annual ASI_E were averaged from the daily values for the period 1981–2018. In order to examine if annual ASI_E is relevant to frequency of '$PM_{2.5}$ pollution weather' episodes, we first calculated the climatological value of the largest 10% of daily ASI_E (i.e. ASI_E_10%) over all grid cells within the entire NC domain and then we used the calculated ASI_E_10% of 8.8 as a single threshold to define '$PM_{2.5}$ pollution weather days' when local daily ASI_E value exceeds the threshold. We obtain the number of 'pollution days' at each grid in a year (shown as a percentage) and the regional average of percentage measures the overall frequency of $PM_{2.5}$ pollution weather days in NC.

2.3. Wave ray tracing (WRT) method

The WRT method, developed from wave kinematics theory, has been used to detect the trajectory of Rossby wave propagation under a specified basic flow field (Li *et al* 2015, 2019). By calculating a cubic

ray equation with a specific starting point and initial wavenumber in the x-direction (i.e. west to east), WRT can compute the energy dispersion pathways of the Rossby wave. The method has been widely adopted to analyze the regional climate change due to global teleconnections (e.g. Shaman and Tziperman 2005, Li *et al* 2015, Scaife *et al* 2017, Li and Ruan 2018).

This study uses WRT to illustrate the physical linkages between the circulation anomalies directly caused by AA emission reduction in Europe and the $PM_{2.5}$ pollution weather variations over China. The key variables for WRT calculation are the ERA5 monthly wind fields at 200 hPa. Following Li *et al* (2019), the climatological wind field was smoothed with the spectral triangular truncation at wavenumber 10 to remove small-scale disturbances.

2.4. Chemistry-climate modeling

We analyze the model outputs from three published large-ensemble model simulations to examine the empirical relationships inferred from observational analysis. The runs are all conducted using the Community Earth System Model version 1 (CESM1; Hurrell *et al* 2013).

(a) CESM1 Large Ensemble (LE) simulations (40 members; Kay *et al* 2015). The CESM1 LE were performed for 1920–2100 with all historical radiative forcing up to 2005 and the Representative Concentration Pathway 8.5 thereafter.
(b) CESM1 simulations with aerosols related to FF in the West region fixed to the 1920 levels when the simulation starts (Fix_WestFF1920; as in Diao *et al* 2021). The West region includes Europe (30°–80° N, 10° W–40° E) and most of North America (20°–80° N, 130°–10° W). All other external forcings evolve from 1920 to 2020 as in CESM1 LE. This ensemble has ten members for 1980–2020.
(c) CESM1 simulations with aerosols related to FF in the East region fixed to the 1920 levels (Fix_EastFF1920; as in Diao *et al* 2021). The setup is the same as Fix_WestFF1920, but only fixing the aerosols over the East (including Asia and portions of Russia, 0–80° N, 60°–150° E). This ensemble has ten members for 1980–2020.

We obtain the climate responses to the regional changes in AA over the West by subtracting the results of the Fix_WestFF1920 from the CESM1 LE, and obtain the responses to the changes in aerosols over the East by subtracting the results of the Fix_EastFF1920 from the CESM1 LE. All results are based on the ensemble average of each run in order to isolate the climate responses to regional AA forcing from model simulated internal variability. Despite the inclusion of AA forcing over North America, figure 1(c) shows that the surface warming caused by the Western AA forcing is mainly located over Europe during 1981–2018, consistent with the larger reduction of AA emissions in Europe (figure 1(a)) and the simulated larger decrease in AOD over Europe (figure 1(b)) compared to North America.

3. Results

3.1. Anti-correlation between European aerosols and ASI_E in NC

The NC is a densely populated and economically developed region, which has experienced the highest concentrations and largest increases of $PM_{2.5}$ in China during the past few decades (supplementary figure 1 (available online at stacks.iop.org/ERL/16/104054/mmedia)). Figure 2(a) shows the changes in ASI_E and percentage of days with larger than ASI_E_10% value averaged over NC for the period 1981–2018. There are fluctuations during certain years: for example, the magnitude of the ASI_E reaches a peak during 2013–2016, when NC experienced frequent and severe $PM_{2.5}$ pollution events (Cai *et al* 2017, Zhong *et al* 2018) despite general emission reduction (Zhang *et al* 2019). Overall, the ASI_E and local $PM_{2.5}$ are correlated (Feng *et al* 2020a). There is a general increase in the ASI_E in NC, indicating that the weather conditions favorable to $PM_{2.5}$ pollution in NC have gone through an interdecadal deterioration. The ASI_E in NC increases at a rate of 6.2% decade^{-1} ($P < 0.001$; relative to the 1981–1985 mean). The largest growth in the ASI_E occurs over places within NC having high air pollutant emissions (Feng *et al* 2020a). The interdecadal trend of the ASI_E is consistent with finding of Zhang *et al* (2018), which defined air quality-related meteorological indices using a different method. There is a high correlation ($r = 0.99$) between the changes in annual mean ASI_E and percentage of days with larger than ASI_E_10%.

During the same period (1981–2018), AA emissions in Europe have decreased significantly (figure 2(b), black line), which has led to an interdecadal decline in the AOD over Europe (figure 2(b), blue line). The larger AODs during 1991–1995 (not shown) are primarily a consequence of the eruption of Mount Pinatubo volcano. Beside those few years, AOD is trending down, in line with the regional SO_2 emission decline. Clearly, there is a strong and intriguing anti-correlation between the increase in the ASI_E or the percentage of days with larger than ASI_E_10% in NC and the decrease in European AA. In particular, there is a sharp decline in AOD or SO_2 emissions but a steady rise in the ASI_E or percentage of days with larger than ASI_E_10% before 2000. The correlation coefficients of ASI_E (percentage of days with larger than ASI_E_10%) are −0.85 (−0.86) and −0.76 (−0.76), with SO_2 emissions and AOD respectively (supplementary table 1), all of which are significant at the 99.9% level. The high correlation could be indicative that

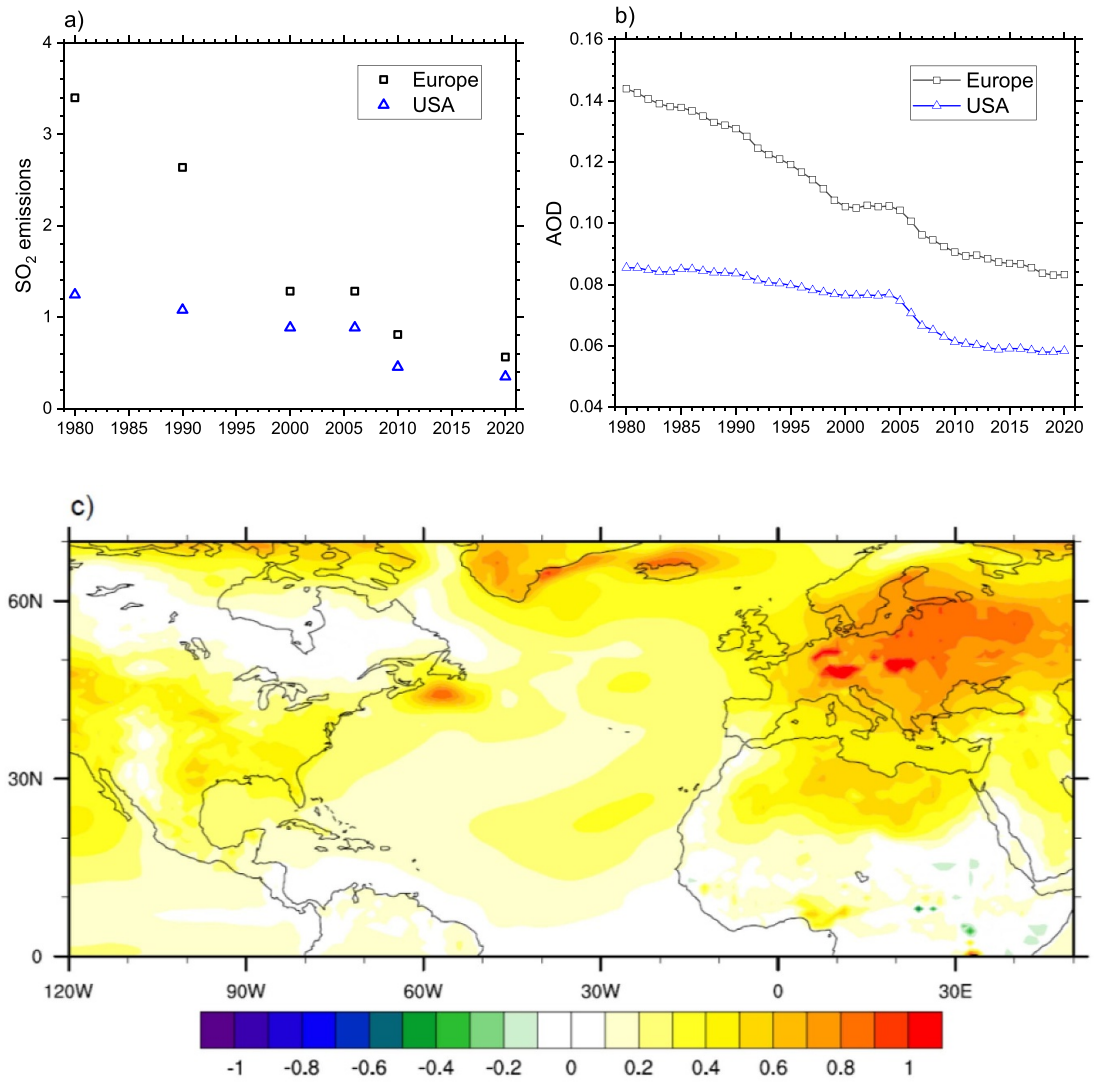

Figure 1. Annual mean (a) SO_2 emissions (unit: g m^{-2}) as the model input to CESM1 LE over Europe (10° W–40° E, 35°–70° N) and USA (130°–60° W, 20°–50° N) and (b) land AOD at 550 nm (unitless) as simulated in the CESM1 LE. (c) Surface air temperature response to changes in aerosol emissions over the West (unit: K (38 year)$^{-1}$) for the period 1981–2018 derived as the difference in trends between CESM1 LE and Fix_WestFF1920 simulations.

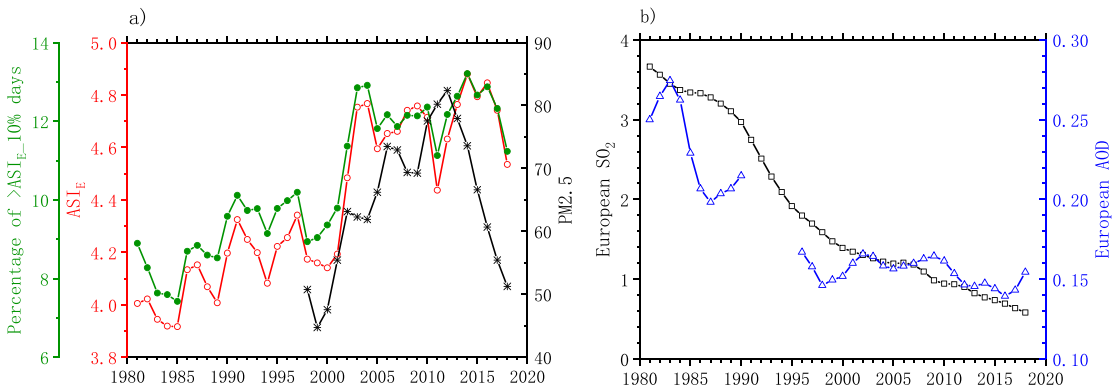

Figure 2. Annual mean (a) ASI_E (red line, unitless), percentage of days with daily value larger than ASI_E_10% (green line, unit: %), and $PM_{2.5}$ concentration (black line, unit: μg m^{-3}) averaged over NC and (b) anthropogenic SO_2 emission (black line, unit: g m^{-2}) and AOD at 550 nm (blue line, unitless) averaged over Europe. Europe is defined as 10° W–40° E, 35°–70° N (black box in figure 3(a)), and NC is defined as 111.9°–119.4° E, 32.5°–41° N (black box in figure 7(c)).

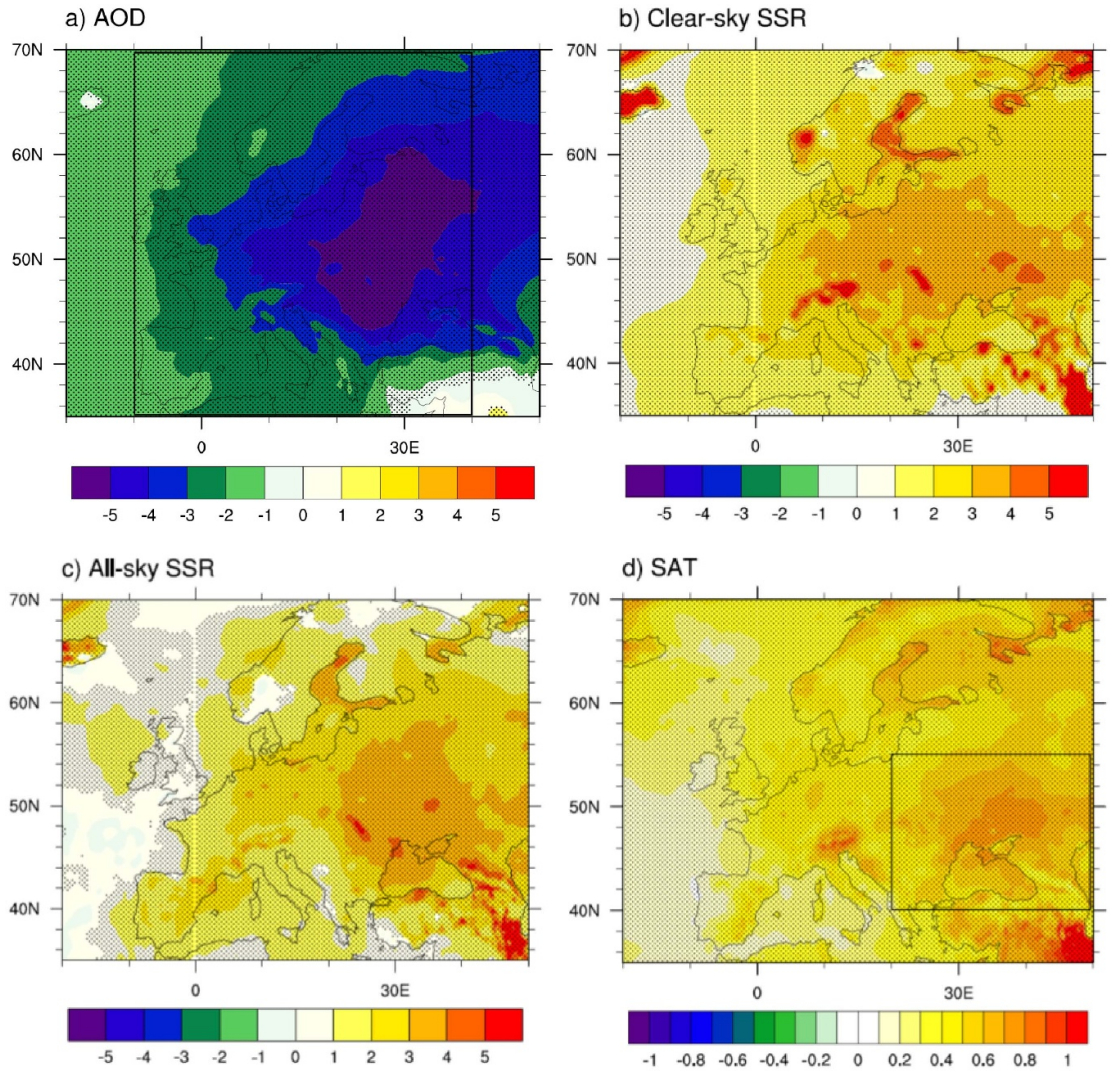

Figure 3. (a) Annual mean AOD trend (unit: 10^{-2} decade^{-1}) from MERRA2. The regression coefficients of annual mean (b) clear-sky and (c) all-sky net SSR fluxes (unit: W m^{-2}) and (d) surface air temperature (SAT, unit: K) from ERA5 with respect to the European SO_2 emissions (1981–2018 time series shown in figure 2(b); unit: g m^{-2}). Note that the regression coefficients in (b)–(d) are flipped in sign (because of the negative trend of SO_2 emission), so that positive values would indicate an increase of corresponding variables in time. Stippling denotes statistical significance at 95%.

the decrease in European aerosol emissions in the recent decades have contributed to the long-term increases in weather conditions in NC conducive to annual mean $PM_{2.5}$ pollutions (ASI_E) and severe pollution episodes (percentage of days with larger than ASI_E_10%). To establish this causality, next we explore the dynamic mechanisms that possibly connect the European aerosol forcing and the $PM_{2.5}$ pollution weather in NC using a regression method.

3.2. Local impact of reduction in European aerosol emissions

Change in aerosol emissions lead to a rapid response in the aerosol burden because of the short residence time (Textor *et al* 2006). There is a downward trend in AOD during 1981–2018 over almost all of Europe (figure 3(a)). The largest decline in AOD is located over central Europe, with a trend exceeding −0.05 decade^{-1}. The decreased AOD lead to a weakening of atmospheric extinction of sunlight due to the interaction of aerosol particles with radiation and clouds, thereby increasing the net flux of surface solar radiation (SSR) (Myhre *et al* 2013). Indeed, the trend of clear-sky and all-sky SSR fluxes over Europe are similar in magnitude and pattern between, when expressed as regression coefficient with respect to the SO_2 emissions over Europe for 1981–2018 (figures 3(b) and (c)). Note that the regression coefficients are flipped in sign so that the positive values here always correspond to an increase in time. The temporal trend of SSR (i.e. simple linear regression with respect to time as done to AOD in figure 3(a)) yields similar results (figures 2(a) and (b)). The largest positive regression coefficients occur over the regions with the largest decline in AOD, especially for the clear-sky SSR (figure 3(b)). There is also a high

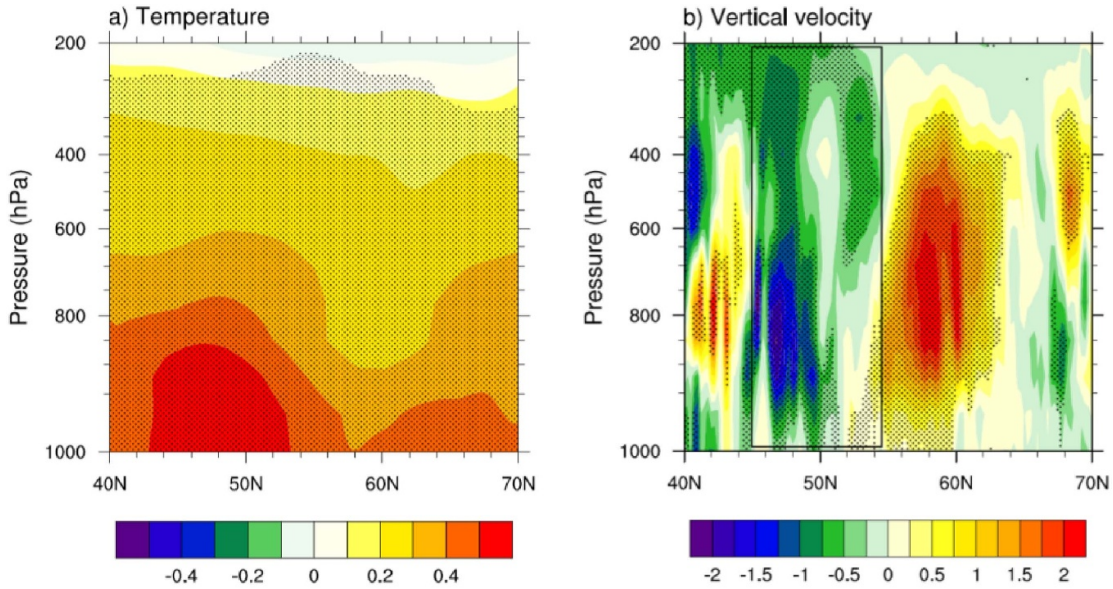

Figure 4. Regressions of zonally averaged (between 20° and 50° E as indicated in the central Europe box in figure 3(d)) (a) temperature (unit: K) and (b) vertical velocity (negative values for upward motion; unit: 10^{-4} Pa s^{-1}) from ERA5 with respect to the European SO_2 emissions (time series in figure 2(b) but with the sign reversed; unit: g m^{-2}). Stippling denotes statistical significance at 95%.

correlation between SSR and AOD or SO_2 emissions in Europe (supplementary table 1). The local surface radiation response is in line with the results in many previous studies that the decreased atmospheric aerosol loadings, rather than cloud changes in response to global warming, have been largely responsible for the surface brightening in Europe since the 1980s (e.g. Wild *et al* 2005, Storelvmo *et al* 2018).

The large and concentrated increase in SSR can lead to local warming at the surface. There is an anomalous warming center over the region of Black Sea (20°–50° E, 40°–55° N; black box in figure 3(d)) when it is regressed upon the SO_2 emissions in Europe, which match the locations of the largest decrease in AOD and the largest positive SSR anomalies (figures 3(a)–(c)). The temporal trends of SSR and surface warming and the simple epoch differences between the two periods of 1999–2018 and 1981–1998 (figures 2 and 3) show consistent patterns with the regression results (figure 3). The regions with the larger temperature response to European sulfate forcing have also been identified in multi-model ensemble simulations of the Precipitation Driver Response Model Intercomparison Project (PDRMIP; Liu *et al* 2018).

The positive surface forcing also warms up the lower atmosphere (figure 4(a)) and as a result, significant updraft anomalies (45°–55° N, black box in figure 4(b)) in the free atmosphere emerge particularly above the warming center with compensating descending motion at both flanks of the warming center (yellow to red regions in figure 4(b)). We further show in figure 5 that such a strong local response in SSR, surface and tropospheric temperature, and atmospheric circulation are all reasonably reproduced in the model experiment with the Western AA emissions as the single forcing, despite a slightly westward maximum center. Furthermore, when the same regression analysis is applied to the historical all-forcing driven CESM LE simulations (supplementary figure 4), we obtain similar results compared to the response derived as the difference between CESM1 LE and Fix_WestFF1920 simulations. Given the robust responses of local radiation, temperature, and circulation to European aerosol forcing as identified in the observational regression analysis and in the model simulations with specifically imposed regional forcings, we ask the next obvious question: what is the consequence downstream?

3.3. Teleconnection between European aerosol emissions and the ASI_E in NC

Figure 6(a) show the annual anomalies of 200 hPa eddy geopotential heights (Z200e) linked to the SO_2 emissions over Europe for the period 1981–2018. The Z200e is defined as the deviation of geopotential height from its zonal mean. The anomalous Z200e over two downstream regions can be statistically connected to the anomalies over Europe in the upper troposphere (black box in figure 6(a)). One of the anomalous wave trains propagates eastward (i.e. the central Europe–Russia–North Pacific pattern, abbreviated as Russia wave train), and the other propagates southeastward from Europe to lower latitudes (i.e. the central Europe–West Asia–northern China–Western Pacific pattern, abbreviated as northern China wave

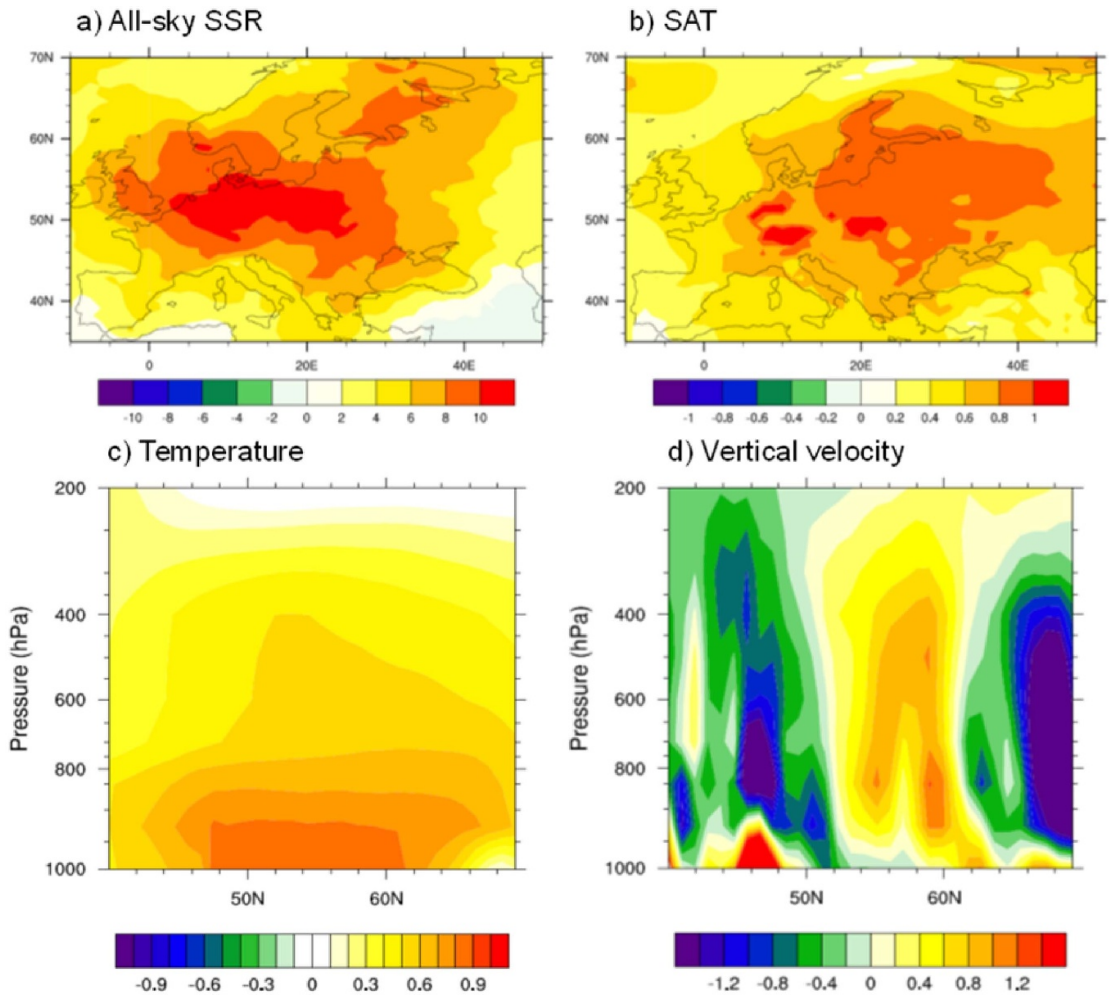

Figure 5. Simulated climate responses to Western aerosol forcing for the period 1981–2018 derived from the differences in trends between CESM1 LE and Fix_WestFF1920. (a) All-sky net SSR flux (unit: W m^{-2} (38 year)$^{-1}$), (b) surface air temperature (unit: K (38 year)$^{-1}$), and zonal averages of (c) atmospheric temperature (unit: K (38 year)$^{-1}$) and (d) vertical velocity (unit: hPa d^{-1} (38 year)$^{-1}$). Zonal average is done between 10° and 40° E, slightly different from figure 4, to follow the simulated local warming center as in figure 5(a).

train) (figure 6(a)). To further illustrate the potential physical connection between the local circulation anomalies in Europe and these downstream anomalies, WRT is used to compute the Rossby wave propagation pathway originating from anomalous Z200e in central Europe to downstream regions (supplementary figure 5). The propagation of the Rossby waves initiated from central Europe regions as directly diagnosed from 200 hPa wind fields follows the same two paths as the regression results based on Z200e revealed in figure 6(a).

The diabatic heating induced anomalous ascending motion over Europe then excited the two anomalous Rossby wave trains across Eurasia, and they can also be identified in the mid to upper troposphere (figure 6(b)), thereby effectively propagating the energy eastward and inducing a downstream response of large-scale circulation. Many earlier studies have identified the importance of diabatic heating in stimulating large-scale wave trains in the extratropics (e.g. Sardeshmukh and Hoskins 1988). The Russia wave train may lead to significant negative anomalous eddy geopotential heights in the upper troposphere of Russia (figure 6(a)). Consequently, the pressure levels drop in the upper troposphere of the region. This increases the poleward and equatorward pressure gradient forces to the south and north of the anomalous Z200e center, respectively (Wang *et al* 2020b). An anomalous cyclone forms over the anomalous negative Z200e through the geostrophic balance between the pressure gradient force and Coriolis force (figure 6(c)), which then leads to an anomalous sinking motion beneath it (50°–55° N) (figure 6(d)). The downward airflow diverges in the lower atmosphere, and an anomalous anticyclone appears at 850 hPa near 50° N (figure 7(b)). As a result, anomalous southeasterly winds to the south of the anticyclone may weaken the cold air intrusion from the higher

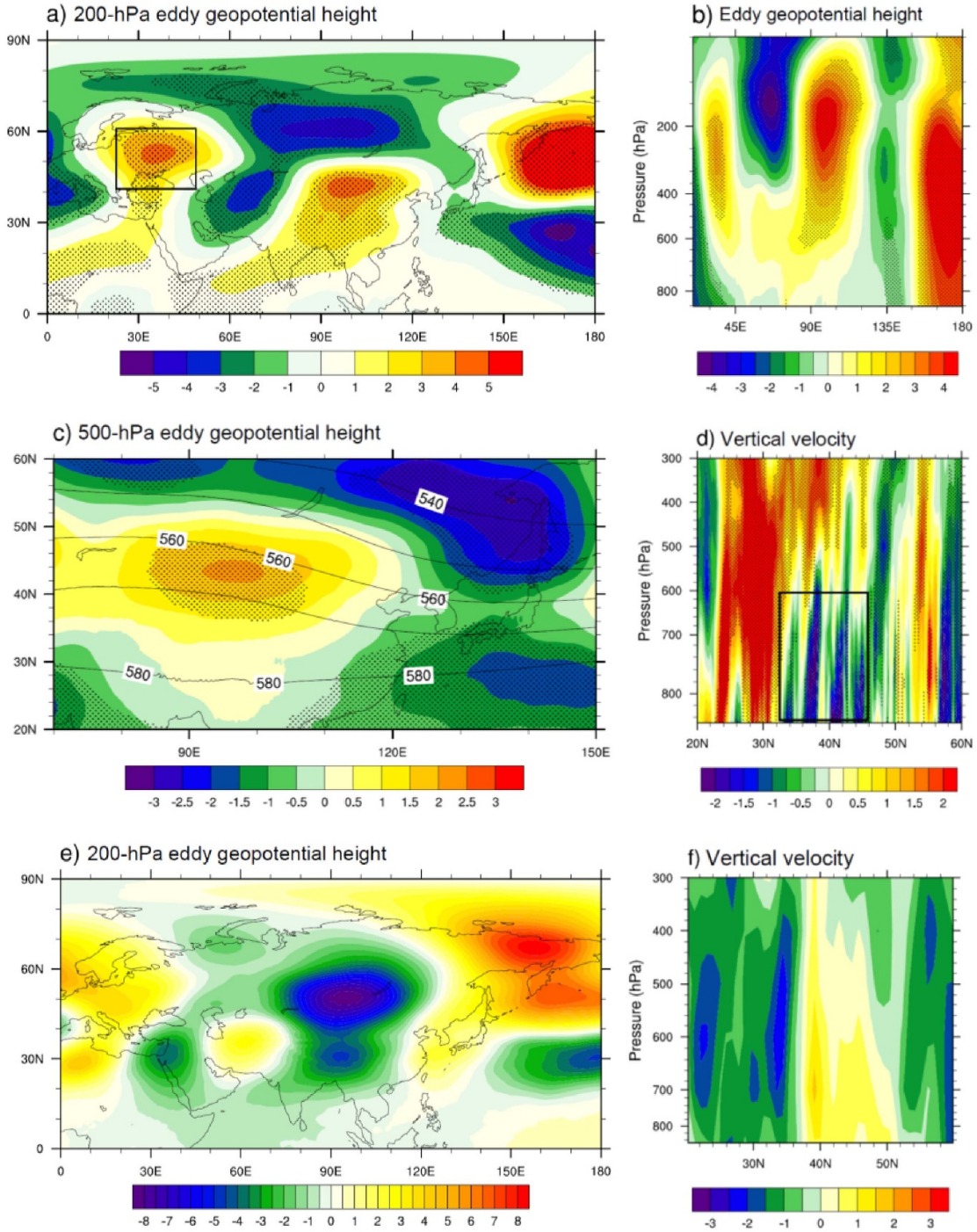

Figure 6. Regressions of (a) 200 hPa eddy geopotential height (unit: m), (b) the profile of eddy geopotential height along 40° N (unit: m), (c) 500 hPa eddy geopotential height (unit: m), and (d) vertical velocity (unit: 10^{-4} Pa s^{-1}) zonally averaged between 110° and 120°E (overlaying North China) from ERA5 upon European SO_2 emissions (sign reversed; unit: g m^{-2}). Note the domain in (c) is smaller than (a) to focus on wave train's projection on China. The contour line in (c) is the climatological geopotential height at 500 hPa (unit: 10 m). Stippling in (a)–(d) denotes statistical significance at 95%. (e) and (f) are simulated responses to Western aerosol forcing (similar to figure 5) for 200 hPa eddy geopotential height (unit: m (38 year)$^{-1}$) and vertical velocity zonally averaged between 110° and 120° E (unit: hPa d^{-1} (38 year)$^{-1}$) to be compared with (a) and (d).

latitudes that serves as a major dispersion driver for air pollution in NC (Zhang *et al* 2018). Indeed, there is a widespread reduction in near-surface wind speeds in large portion of NC (figure 7(c)).

The northern China wave train may result in significant positive anomalous eddy geopotential heights in the upper troposphere of northern China and Mongolia (figures 6(a) and (b)). Thus, there are increases in equatorward and poleward pressure gradient forces to the south and north of the anomalous positive Z200e center, respectively. This leads to an anomalous anticyclone in the upper troposphere of those regions and an anomalous ascending motion beneath it (32°–45° N) (black box in figure 6(d)). The enhanced upward motion generates positive anomalous eddy geopotential heights at 500 hPa over

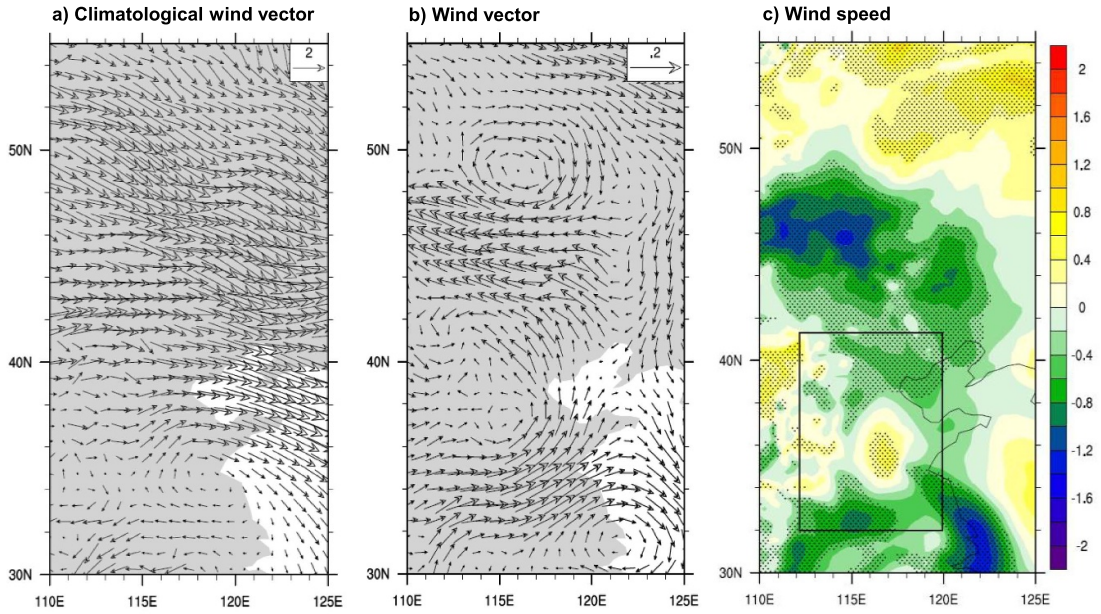

Figure 7. (a) Climatological wind vector averaged between 850 and 1000 hPa (unit: m s^{-1}) during 1998–2018 and regressions of (b) wind vector at 850 hPa and (c) wind speed averaged between 850 and 1000 hPa (unit: 10 m s^{-1}) from ERA5 upon the European SO_2 emissions (sign reversed; unit: g m^{-2}). Black box in (c) is the NC region. Stippling in (c) denotes statistical significance at 95%.

the northern China–Mongolia region (figure 6(c)), thereby weakening the East Asian trough. Correspondingly, an anomalous cyclone forms at 850 hPa in eastern China between 32° N and 45° N (figure 7(b)) due to the enhanced ascending motion. This can lead to anomalous southerly winds in the lower atmosphere in the coastal areas of NC, and further intensifies the southeasterly wind anomalies (figure 7(b)) and weakens the near-surface wind speeds in NC (figure 7(c)) that are prevailingly northwesterly (figure 7(a)).

To test the dynamic mechanisms inferred from observational regression analysis, we further examine the simulated responses to aerosol forcing in Europe and North America derived as the difference between a pair of model experiments (see section 2). The model results essentially support the mechanisms suggested by regression analysis (figures 6(e) and (f)). Consistently, there are also two anomalous Rossby wave trains across Eurasia in the upper troposphere (figure 6(e)) due to the only perturbation of the aerosol forcing over the West, rather than global warming or internal variability. Compared to the regression results, the Russia pattern is reasonably reproduced, while the northern China pattern lies more southeastward. As a result, the simulated anomalous ascending motion (figure 6(f)) is further at the south of NC compared to the observation. A more concrete modeling evidence is the simulated increasing trends of 0.1–0.5 μg m^{-3} (38 year)$^{-1}$ in surface sulfate concentration and of 0.001–0.006 (38 year)$^{-1}$ in AOD in most of NC (figures 8(a) and (b)), despite invariant local aerosol emissions. However, the increases in sulfate and AOD levels in NC in response to the decrease in European aerosols are an order of magnitude smaller than those in response to the increase in Asian aerosols (figures 8(c), (d) and supplementary figure 6). This, unsurprisingly, indicates that the significant increase in AA emissions is the main cause of long-term increase in $PM_{2.5}$ pollution in China (An *et al* 2019). Comparing the changes driven by meteorology and driven by local emissions (figure 8 top row vs bottom row) help contextualize the influence of the proposed teleconnection mechanism here, which plays a relatively small but non-negligible role.

The teleconnection patterns have a potential for weakening the horizontal dispersion of air pollutants in NC. Indeed, the long-term increase in the ASI_E in NC is found to be primarily due to the decreases in near-surface wind speeds (i.e. horizontal ventilation) and decrease in PBL height (in MERRA-2; Feng *et al* 2020a). Other studies also reported that $PM_{2.5}$ pollution over NC is often accompanied by anomalous southerly winds in the lower atmosphere, decreased wind speeds, and a weakened East Asian trough (Chen and Wang 2015). The teleconnection can also suppress the downward transport of westerly momentum in NC, which not only preserves the inversion boundary layer but also blocks the dry and clean air from the upper levels (Yin *et al* 2021).

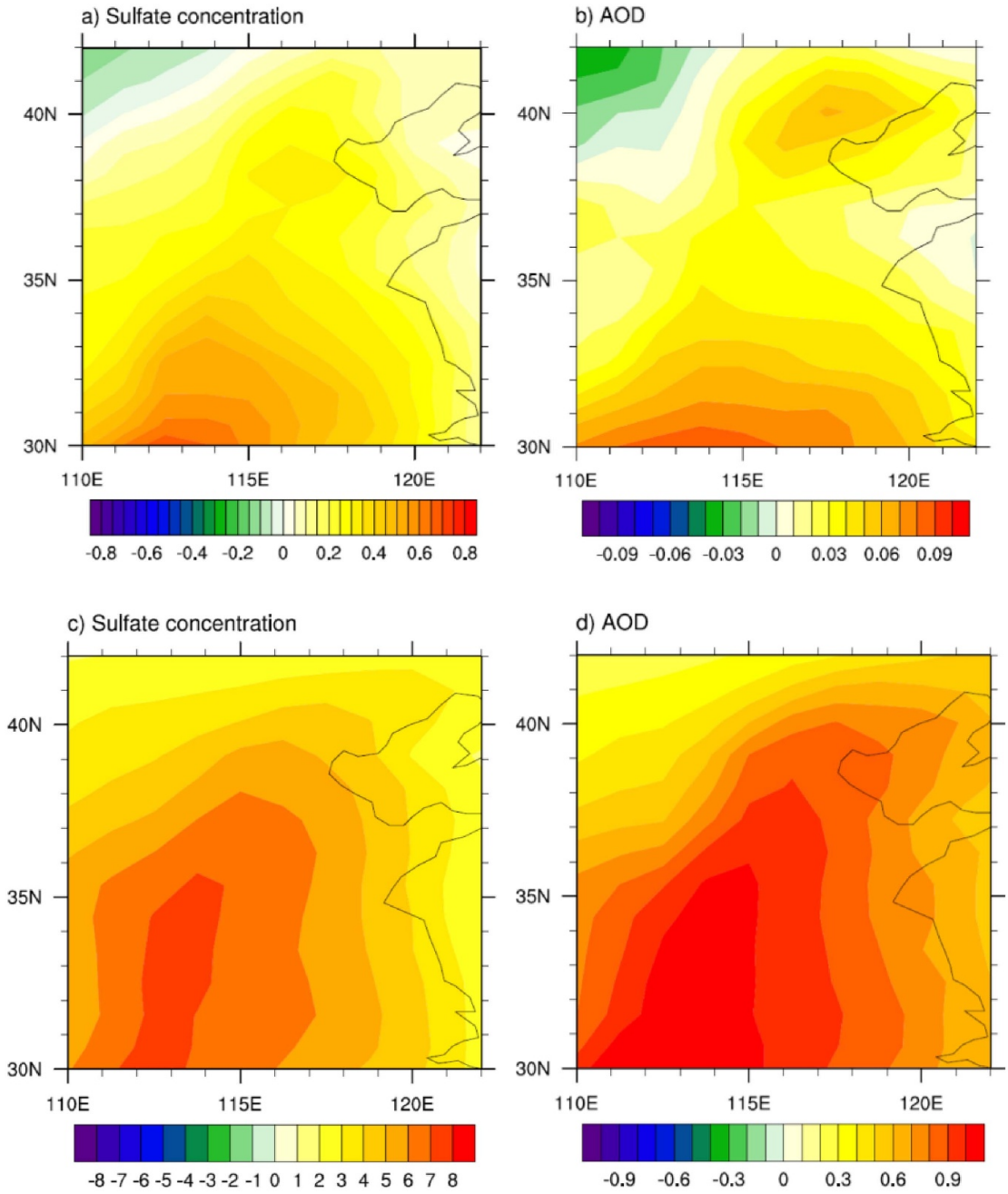

Figure 8. Simulated changes of (a), (c) surface sulfate concentrations (unit: μg m^{-3} (38 year)$^{-1}$) and (b), (d) AOD (unit: 10^{-1} (38 year)$^{-1}$) in NC in response to changes in aerosol emissions over the West derived as the differences in trends between CESM1 LE and Fix_WestFF1920 (a), (b) and over the East derived as the differences in trends between CESM1 LE and Fix_EastFF1920 (c), (d). Note that the magnitude of change in (a), (b) is smaller than in (c), (d). The trends of sulfate concentrations in these three runs are shown globally in supplementary figure 6 for references.

4. Conclusions and discussions

We examine a potential linkage of decreased European AA emissions and the weather conditions conducive to $PM_{2.5}$ pollution in NC for the period 1981–2018. Our results show that the decreased European AA emissions since the 1980s may have partially contributed to the interdecadal increase in both weather conditions in NC conducive to annual average $PM_{2.5}$ pollution (ASI_E) and severe pollution episodes (percentage of days with larger than ASI_E_10%), primarily by modulating atmospheric circulation patterns across Eurasia (figure 9). Our regression analysis suggests that the decreased European AA emissions may explain the increase in SSR and the lower atmosphere warming over Europe. Two anomalous Rossby wave trains in the upper troposphere are stimulated across Eurasia due to the enhanced local diabatic heating and anomalous ascending motion in Europe. The teleconnection patterns then weaken the near-surface horizontal dispersion in NC, which may be favorable

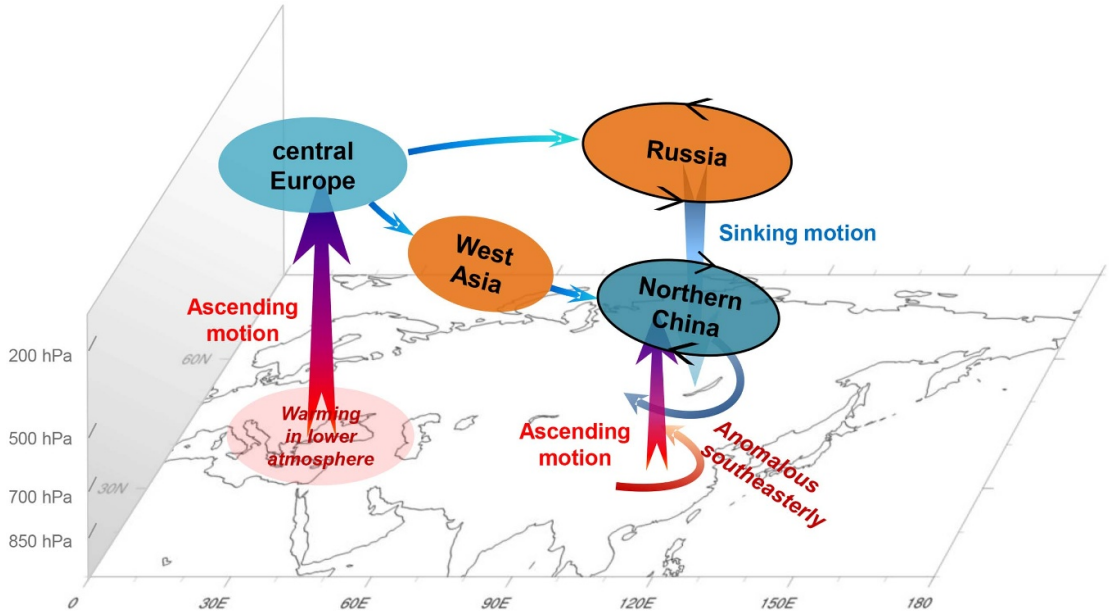

Figure 9. Schematic of the dynamic mechanisms connecting the European AA reduction and the weather conditions conducive to $PM_{2.5}$ pollution in NC.

to the increase in local ASI_E and air pollution build-up.

The suggested mechanism is further supported by the results from a pair of large-ensemble simulations with AA changes over the West as the single forcing, which is shown to excite similar local heating and ascending motion over Europe and West-to-East teleconnection patterns (despite a slightly different maximum center), and to increase the sulfate levels in NC. The regression analysis on CESM1 LE simulations driven by all historical forcing provides more supporting evidence that the regression analysis applied to reanalysis, while not conclusive, is indicative of some causal relationship. However, it should be emphasized that the significant increase in local AA emissions is the primary cause of long-term increase in $PM_{2.5}$ pollution in China.

Overall, the proposed causality is motivated from the strong correlation as indicated in figure 2 and supplementary table 1, and it is further strengthened by multiple lines of evidence: (a) statistical analyses that suggest the physical mechanisms connecting local heating in Europe to the circulation anomaly over NC favorable to local pollution build up; (b) the model sensitivity experiments in which the European aerosol reduction is introduced as the perturbation and yields a similar response, not only in the simulated dynamical fields but also in the simulated PM and AOD levels over NC; and (c) the same type of regression analysis applied to the historical model runs (supplementary figure 4), which produces qualitatively similar linkage demonstrated by the control-perturbation analysis in (b).

The implication of this study is multifold. This proposed 'West-to-East Aerosol-to-Aerosol' teleconnection mechanism helps resolve opposite views on the impact of global and local air pollution on $PM_{2.5}$ pollution weather in NC (i.e. Hong *et al* 2020 , Feng *et al* 2020b). Europe is continuing to improve air quality, which will undoubtedly lead to a sustained decline of AA emissions in coming decades (Gidden *et al* 2019). Our results also imply that the remote climate response to future decreases in European AA emissions could partially offset the benefits of air quality improvement measures in NC.

Because of the distinct climate responses to AA in different models (Liu *et al* 2018), we acknowledge that similar dedicated model experiments from other chemistry-climate models should be conducted and closely examined to further test the hypotheses here. Ideally, some dedicated runs should be performed with single forcing of 1980–2020 aerosol changes (in the West and in the East) to avoid the practice of subtraction in deriving climate response as done here. This additional test is useful because in principle, the different background climate conditions could affect how the local PM concentrations over China respond to remote aerosol forcing over Europe.

Note that the reduction in European AA affects the $PM_{2.5}$ pollution in China through both the decreased aerosol transport (although weak as indicated in figure 6(c)) and the increased ASI_E. To fully separate the two factors, there is a need to conduct dedicated model experiments with meteorological and chemical fields separately prescribed to a regional chemistry-climate model over China. These too can be important research efforts using multiple models.

Data availability statement

The ERA5 data from the European Centre for Medium-Range Weather Forecasts are available at https://cds.climate.copernicus.eu/#!/search?text=ERA5%26type=dataset. The historical and future SO_2 emissions are from the CEDS and under the SSP2-4.5, respectively, available at https://tntcat.iiasa.ac.at/SspDb/dsd?Action=htmlpage&page=20. The AOD data from MERRA-2 are available at https://disc.gsfc.nasa.gov/daac-bin/FTPSubset2.pl. The $PM_{2.5}$ surface concentrations are available at http://fizz.phys.dal.ca/~atmos/martin/?page_id=140.

The data that support the findings of this study are openly available at the following URL/-DOI: https://cds.climate.copernicus.eu/cdsapp#!/dataset/reanalysis-era5-pressure-levels-monthly-means?tab=form.

Acknowledgments

This study was supported by the National Natural Science Foundation of China (41875179, 41705135, and 42090032), Basic Research Fund of CAMS (2019Z014), and science and technology development fund of CAMS (2021KJ010). We appreciate the comments from three anonymous reviewers.

ORCID iDs

Zhili Wang https://orcid.org/0000-0002-4392-3230
Jin Feng https://orcid.org/0000-0003-4454-5785
Yangyang Xu https://orcid.org/0000-0001-7173-7761

References

Acosta Navarro J C, Varma V, Riipinen I, Seland Ø, Kirkevåg A, Struthers H, Iversen T, Hansson H-C and Ekman A M L 2016 Amplification of Arctic warming by past air pollution reductions in Europe *Nat. Geosci.* **9** 277–81

An Z *et al* 2019 Severe haze in northern China: a synergy of anthropogenic emissions and atmospheric processes *Proc. Natl Acad. Sci. USA* **116** 8657–66

Bollasina M A, Ming Y and Ramaswamy V 2011 Anthropogenic aerosols and the weakening of the South Asian summer monsoon *Science* **334** 502–5

Cai W, Li K, Liao H, Wang H and Wu L 2017 Weather conditions conducive to Beijing severe haze more frequent under climate change *Nat. Clim. Change* **7** 257–62

Chen H and Wang H 2015 Haze days in North China and the associated atmospheric circulations based on daily visibility data from 1960 to 2012 *J. Geophys. Res. Atmos.* **120** 5895–909

Cohen A J *et al* 2017 Estimates and 25-year trends of the global burden of disease attributable to ambient air pollution: an analysis of data from the global burden of diseases study 2015 *Lancet* **389** 1907–18

Diao C, Xu Y and Xie S-P 2021 Anthropogenic aerosol effects on tropospheric circulation and sea surface temperature (1980–2020): separating the role of zonally asymmetric forcings *Atmos. Chem. Phys. Discuss.* (https://doi.org/10.5194/acp-2021-407)

Ding A J *et al* 2016 Enhanced haze pollution by black carbon in megacities in China *Geophys. Res. Lett.* **43** 2873–9

Ding Y and Liu Y 2014 Analysis of long-term variations of fog and haze in China in recent 50 years and their relations with atmospheric humidity *Sci. China Earth Sci.* **57** 36–46

Feng J, Liao H, Li Y, Zhang Z and Tang Y 2020a Long-term trends and variations in haze-related weather conditions in north China during 1980–2018 based on emission-weighted stagnation intensity *Atmos. Environ.* **240** 117830

Feng J, Quan J, Liao H, Li Y and Zhao X 2018 An air stagnation index to qualify extreme haze events in northern China *J. Atmos. Sci.* **75** 3489–505

Feng W, Wang M, Zhang Y, Dai X, Liu X and Xu Y 2020b Intraseasonal variation and future projection of atmospheric diffusion conditions conducive to extreme haze formation over eastern China *Atmos. Ocean. Sci. Lett.* **13** 346–55

Gao M, Carmichael G R, Wang Y, Saide P E, Yu M, Xin J, Liu Z and Wang Z 2016 Modeling study of the 2010 regional haze event in the North China Plain *Atmos. Chem. Phys.* **16** 1673–91

Gidden M J *et al* 2019 Global emissions pathways under different socioeconomic scenarios for use in CMIP6: a dataset of harmonized emissions trajectories through the end of the century *Geosci. Model Dev.* **12** 1443–75

Hammer M S *et al* 2020 Global estimates and long-term trends of fine particulate matter concentrations (1998–2018) *Environ. Sci. Technol.* **54** 7879–90

Hersbach H *et al* 2020 The ERA5 global reanalysis *Q. J. R. Meteorol. Soc.* **146** 1999–2049

Hoesly R M *et al* 2018 Historical (1750–2014) anthropogenic emissions of reactive gases and aerosols from the Community Emissions Data System (CEDS) *Geosci. Model Dev.* **11** 369–408

Hong C, Zhang Q, Zhang Y, Davis S J, Zhang X, Tong D, Guan D, Liu Z and He K 2020 Weakening aerosol direct radiative effects mitigate climate penalty on Chinese air quality *Nat. Clim. Change* **10** 845–50

Hurrell J W *et al* 2013 The community earth system model: a framework for collaborative research *Bull. Am. Meteorol. Soc.* **94** 1339–60

Kay J E *et al* 2015 The Community Earth System Model (CESM1) large ensemble project: a community resource for studying climate change in the presence of internal climate variability *Bull. Am. Meteorol. Soc.* **96** 1333–49

Lamarque J-F *et al* 2010 Historical (1850–2000) gridded anthropogenic and biomass burning emissions of reactive gases and aerosols: methodology and application *Atmos. Chem. Phys.* **10** 7017–39

Lau W K M 2016 The aerosol-monsoon climate system of Asia: a new paradigm *J. Meteorol. Res.* **30** 1–11

Lewinschal A, Ekman A M L, Hansson H-C, Sand M, Berntsen T K and Langner J 2019 Local and remote temperature response of regional SO_2 emissions *Atmos. Chem. Phys.* **19** 2385–403

Li J and Ruan C 2018 The North Atlantic–Eurasian teleconnection in summer and its effects on Eurasian climates *Environ. Res. Lett.* **13** 024007

Li Y, Feng J, Li J and Hu A 2019 Equatorial windows and barriers for stationary Rossby wave propagation *J. Clim.* **32** 6117–35

Li Y, Li J, Jin F and Zhao S 2015 Interhemispheric propagation of stationary Rossby waves in a horizontally nonuniform background flow *J. Atmos. Sci.* **72** 3233–56

Liu L *et al* 2018 A PDRMIP multimodel study on the impacts of regional aerosol forcings on global and regional precipitation *J. Clim.* **31** 4429–47

Myhre G *et al* 2017 PDRMIP: a precipitation diver and response model intercomparison project, protocol and preliminary results *Bull. Am. Meteorol. Soc.* **98** 1185–98

Myhre G *et al* 2013 Anthropogenic and natural radiative forcing *Climate Change 2013: The Physical Science Basis.*

Contribution of Working Group I to the Fifth Assessment Report of the Intergovernmental Panel on Climate Change ed T F Stocker *et al* (Cambridge: Cambridge University Press) Ch 8, pp 659–740

Pope C A and Dockery D W 2006 Health effects of fine particulate air pollution: lines that connect *J. Air Waste Manage. Assoc.* **56** 709–42

Rao S *et al* 2017 Future air pollution in the Shared Socio-economic Pathways *Glob. Environ. Change* **42** 346–58

Rich D Q *et al* 2012 Association between changes in air pollution levels during the Beijing Olympics and biomarkers of inflammation and thrombosis in healthy young adults *JAMA* **307** 2068–78

Sardeshmukh P D and Hoskins B J 1988 The generation of global rotational flow by steady idealized tropical divergence *J. Atmos. Sci.* **45** 1228–51

Scaife A A *et al* 2017 Tropical rainfall, Rossby waves and regional winter climate predictions *Q. J. R. Meteorol. Soc.* **143** 1–11

Shaman J and Tziperman E 2005 The effect of ENSO on Tibetan Plateau snow depth: a stationary wave teleconnection mechanism and implications for the South Asian monsoons *J. Clim.* **18** 2067–79

Storelvmo T, Heede U K, Leirvik T, Phillips P C B, Arndt P and Wild M 2018 Lethargic response to aerosol emissions in current climate models *Geophys. Res. Lett.* **45** 9814–23

Textor C *et al* 2006 Analysis and quantification of the diversities of aerosol life cycles within AeroCom *Atmos. Chem. Phys.* **6** 1777–813

Wang Y, Le T, Chen G, Yung Y L, Su H, Seinfeld J H and Jiang J H 2020a Reduced European aerosol emissions suppress winter extremes over northern Eurasia *Nat. Clim. Change* **10** 225–30

Wang Z *et al* 2021 Weakened aerosol-PBL interaction during COVID-19 lockdown in northern China *Geophys. Res. Lett.* **48** e2020GL090542

Wang Z, Mu J, Yang M and Yu X 2020b Reexamining the mechanisms of East Asian summer monsoon changes in response to non-East Asian anthropogenic aerosol forcing *J. Clim.* **33** 2929–44

Wild M *et al* 2005 From dimming to brightening: decadal changes in solar radiation at Earth's surface *Science* **308** 847–50

Wu G *et al* 2016 Advances in studying interactions between aerosols and monsoon in China *Sci. China Earth Sci.* **59** 1–16

Yin Z, Zhou B, Chen H and Li Y 2021 Synergetic impacts of precursory climate drivers on interannual-decadal variations in haze pollution in North China: a review *Sci. Total Environ.* **755** 143017

Yu X, Wang Z, Zhang H and Zhao S 2019 Impacts of different types and intensities of El Niño events on winter aerosols over China *Sci. Total Environ.* **655** 766–80

Zhang Q *et al* 2019 Drivers of improved $PM_{2.5}$ air quality in China from 2013 to 2017 *Proc. Natl Acad. Sci. USA* **116** 24463–2446

Zhang X, Zhong J, Wang J, Wang Y and Liu Y 2018 The interdecadal worsening of weather conditions affecting aerosol pollution in the Beijing area in relation to climate warming *Atmos. Chem. Phys.* **18** 5991–9

Zhong J, Zhang X, Dong Y, Wang Y, Liu C, Wang J, Zhang Y and Che H 2018 Feedback effects of boundary-layer meteorological factors on cumulative explosive growth of $PM_{2.5}$ during winter heavy pollution episodes in Beijing from 2013 to 2016 *Atmos. Chem. Phys.* **18** 247–58

Zou Y, Wang Y, Zhang Y and Koo J-H 2017 Arctic sea ice, Eurasia snow, and extreme winter haze in China *Sci. Adv.* **3** e1602751